10.1109/ULTSYM.2009.0015

In Vivo Treatment of Rabbit VX2 Tumor by Miniaturized Image-Ablate Ultrasound Arrays

T. Douglas Mast*, Peter G. Barthe†, Inder Raj S. Makin†, Michael H. Slayton†, Chandra Priya Karunakaran*, Mark T. Burgess*, Amel Alqadah*, Joseph F. Buell‡, and Steven M. Rudich§
*Department of Biomedical Engineering, University of Cincinnati, Cincinnati, Ohio
†Guided Therapy Systems/Ardent Sound, Mesa, Arizona
‡Department of Surgery, University of Louisville, Louisville, Kentucky
§Department of Surgery, University of Cincinnati, Cincinnati, Ohio

***Abstract*—In the preclinical studies reported here, VX2 cancer within rabbit liver has been treated by bulk ultrasound ablation employing miniaturized image-ablate arrays. Array probes were constructed with 32 elements in a 2.3×20 mm^2 aperture and employed for B-scan imaging as well as bulk ablation at 4.8 MHz. In a series of *in vivo* experiments, tumor ablation using these arrays was histologically confirmed, with complete ablation of tumor cross sections for exposures with delivery of >747 J acoustic energy. These results show feasibility for development of an image-guided, interstitial bulk ultrasound ablation approach for clinical liver cancer treatment.**

I. Introduction

Minimally-invasive ultrasound ablation, which employs small transducer elements deployed interstitially or laparoscopically, has the potential to provide highly selective treatment with improved image guidance compared to radiofrequency ablation, without the complexity of extracorporeal focused ultrasound approaches [1]. Work in this area has included interstitial ultrasound therapy employing unfocused [2] as well as weakly focused [3] elements. Multiple-element arrays allow greater treatment selectivity by allowing switching and limited focusing [4]–[6].

Recent work on minimally-invasive ultrasound ablation technology has included development and testing of miniaturized arrays capable of both imaging and ablation in minimally-invasive, laparoscopic or interstitial configurations. Use of the same array elements for both imaging and ablation can provide ultrasound power delivery suitable for rapid volume ablation, as well as high-quality imaging [4], [6]. This approach is capable of treating large tumors at speeds comparable to RF ablation, but with greater spatial selectivity. Treatment planning and monitoring can also be improved, since the imaged volume is identical to the treated volume.

In an approach recently proposed for treatment of liver cancer [6], an ultrasound probe capable of both B-scan imaging and intense ultrasound ablation is inserted into soft tissue using a percutaneous, laparoscopic, or open surgical approach. The probe is used to image the tumor and surrounding tissue, allowing user planning of an bulk ablation procedure. Thermal ablation of a tissue volume is then performed using electronic scanning and mechanical probe rotation. The present study demonstrates feasibility for *in vivo* cancer ablation using 4.8 MHz image-ablate ultrasound array probes designed for interstitial deployment.

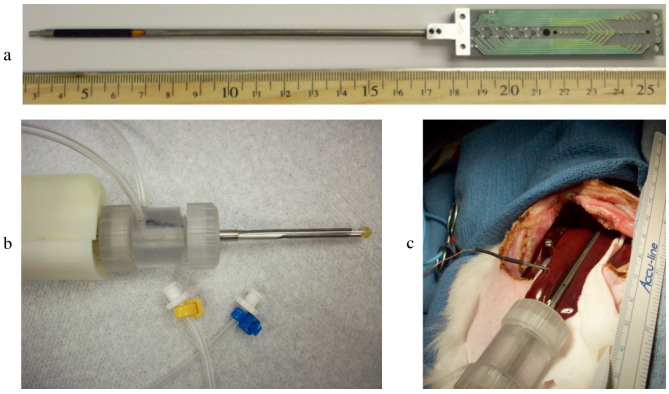

Fig. 1: Miniaturized image-ablate ultrasound probe. (a) THX4A array device showing 32 element, 20 mm aperture, 8-gauge needle housing, and interconnect board. (b) Assembled probe with handpiece, PET coupling balloon, and circulation connections. (c) Probe placed for ablation of rabbit liver *in vivo*.

II. Materials and Methods

A. Image-ablate ultrasound probes

Image-ablate ultrasound probes have been designed and constructed to optimize array performance under constraints relevant for clinical implementation of interstitial ultrasound ablation. A maximum shaft diameter of 3.125 mm (8-gauge) for interstitial deployment allows, according to our previous experience [6], active array dimensions of about 2.3 mm in elevation and a channel count of 32 elements.

Given these constraints, simulations were undertaken to determine the optimal aperture size and frequency for our image-ablate arrays. Heat deposition, defined as the locally absorbed ultrasound power per unit tissue volume and unit surface intensity, was computed for ranges of possible probe dimensions, frequencies, and focus positions using an accurate model for diffracted ultrasound fields [7]. This model was applied to simulate heat deposition in liver tissue using previously validated methods for numerical solution of the Pennes bio-heat transfer equation [8]. These methods take into account ultrasound diffraction and frequency-dependent absorption, heat conduction, perfusion-induced losses, tissue

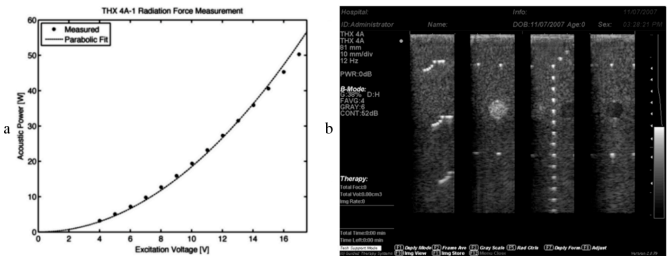

Fig. 2: THX4A image-ablate array test results. (a) Acoustic power measured by a radiation-force balance, plotted vs. driver voltage for full aperture, 4.8 MHz sonication. (b) B-scan images of a standard quality-assurance phantom, showing achievable contrast and resolution vs. image depth.

modification caused by thermal ablation, and redistribution of heat in the presence of tissue vaporization.

Ablation depth and rate were computed as a function of aperture length and sonication frequency, for array configurations with 2.3 mm elevation, 32 elements, and electronic focusing corresponding to capabilities of the Iris 2 imaging and ablation system [9]. Optimization results indicated that a center frequency of 4.8 MHz and aperture length of 20 mm would provide ablation meeting performance targets, including thermal lesion depths $\geq$20 mm (corresponding to 4 cm diameter lesion volumes), ablation rates $\geq$1 ml/min, and beam widths suitable for B-scan imaging.

Design and fabrication of image-ablate arrays with 32 elements and a pitch of 0.625 mm selected to satisfy the clinical requirements of size, ablation rate, and imaging performance. The resulting device, called the THX4A array, is shown in Fig. 1(a). Materials used were an air-backed, PZT-4 equivalent piezoelectric ceramic with composite matching layer ground to a quarter-wavelength thickness and diced and bussed into array elements. The array housing design is a machined stainless-steel tube.

For preclinical testing, a prototype probe design incorporated a cooling and coupling system for the THX4A image-ablate array probe. In this circulation system [Fig. 1(b)], the 3 mm array fits securely within a 4.9 mm OD, 64 μm wall thickness PET tube, heat-shrunk at 375 °C and affixed to a tissue-piercing polyimide end cap. This tube is interfaced to a custom-designed manifold with Luer-lock fittings for interfacing with an external circulation apparatus. Deionized, degassed water is chilled to 5-10 °C (Centrivap cold trap) and circulated by a peristaltic pump (Harvard Apparatus) at a rate of 60 ml/min. The array and circulation apparatus are connected to an integrated cable and handpiece that interface with the Iris 2 system for controlled imaging and ablation.

Performance test results for a typical THX4A array are shown in Fig. 2. A calibrated radiation-force-balance acoustic power meter (Ohmic Instruments UPM-1) was used to characterize the array driven from an RF amplifier and source (ENI A150, Agilent 33250A). Fig. 2(a) shows that for 4.8 MHz sonication, as used in the ablation studies described below, greater than 50 W continuous acoustic power output is achievable within the normal operating range of the probe. This corresponds to >110 W/cm^2 acoustic intensity at the probe

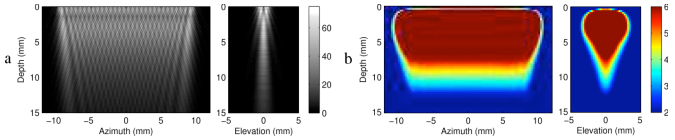

Fig. 3: Simulated tissue ablation performance for THX4A probe in a representative treatment scenario (4.8 MHz, 20 mm unfocused aperture, 32 W/cm^2 surface intensity, 60 s sonication, 85% duty, *in vivo* perfusion conditions). (a) Simulated *in situ* intensity, showing azimuth (array direction) and elevation planes. (b) Cumulative thermal dose after 60 s ($\log_{10}$[EM43]), with thermal lesioning predicted for 200 equivalent minutes at 43 °C, or $\log_{10}$[EM43] $\geq$2.3.

surface. Comparable power output is also available at a second therapeutic frequency of 3.5 MHz.

The THX4A elements are also capable of pulse-echo imaging, with a fractional bandwidth of 50% at a center frequency of 4.4 MHz. The resulting image quality is illustrated in Fig. 2(b), which shows B-scans obtained using a THX4A array with the prototype Iris 2 imaging-ablation platform [9]. These images of a standard ultrasound quality assurance phantom (ATS) show good contrast and detail resolution, comparable to larger conventional imaging arrays. The finer acoustic pitch of 1.79λ, in comparison to 3.4λ for first-generation probes [6], improves imaging in terms of beam steering and focusing capability, as well as detail and contrast resolution.

B. Ablation exposure conditions

The THX4A arrays were designed with two possible frequencies for high-intensity, therapeutic sonication, 3.5 MHz and 4.8 MHz. At either frequency, the THX4A arrays are capable of high-intensity sonication, with surface acoustic intensities >110 W/cm^2 [Fig. 2(a)]. Exposure conditions for *in vivo* ablation using the THX4A arrays were guided, within these constraints, by simulations employing the numerical methods described above [8].

Appropriate exposure conditions, capable of ablating large tissue volumes in the perfused liver environment, were determined in simulations to be an unfocused, 32-element (20 mm) aperture firing at 4.8 MHz with surface intensities in the range 20-40 W/cm^2 for durations 1-2 min. Simulated results are shown in Fig. 3 for a typical ablation exposure within this range, resulting in ablation of 1.2 ml liver tissue in 1 min. Exposure conditions were further confirmed by *in vitro* ablation experiments before undertaking the preclinical *in vivo* cancer ablation studies described below.

C. VX2 liver cancer model

In order to effectively test feasibility of liver cancer ablation by these image-ablate ultrasound devices, a liver cancer model for bulk ultrasound ablation has been implemented. This was based on the VX2 carcinoma in rabbit liver, which has been previously employed in studies of radiofrequency and HIFU ablation therapies [10]–[12]. Preliminary work on this model has verified that tumors can be consistently grown to a size suitable for tests of image-guided bulk ultrasound ablation. After implantation of tumor cells (one tumor fragment in each of the left, medial and right lobes of the rabbit liver)

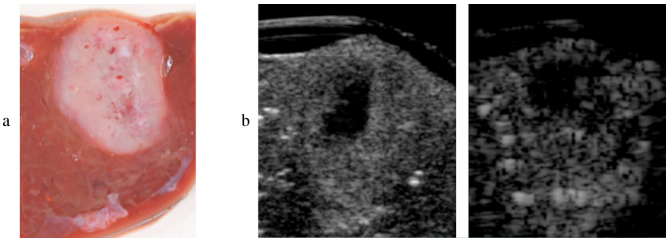

Fig. 4: VX2 liver cancer model. (a) Cross section of untreated VX2 tumor stained by TTC, with pink appearance indicating cell viability. (b) *In vitro* B-scan images of VX2 tumor in rabbit liver. Left: B-scan from 192-element, 7 MHz, diagnostic-quality linear array, 48 dB dynamic range. Right: B-scan from a 32-element, 4 MHz image-ablate array, 60 dB dynamic range.

and 11–14 days growth, tumors reliably grow to solid masses of 0.9 ± 0.3 cm diameter. The resulting tumors (three per animal) can then be effectively imaged and ablated using our miniaturized ultrasound arrays (Figs. 4 and 5). Longer tumor growth results in tumors with necrotic, liquified cores unsuitable for histologic evaluation, with diameters 1.9 ± 0.5 for 21 days growth.

Thermal coagulation caused by bulk ultrasound ablation *in vivo* can be effectively evaluated, both in VX2 tumor and surrounding liver parenchyma, using histologic and vital staining techniques. As illustrated in Figs. 4 and 5, a vital stain suitable to quantify volumetric ablation is triphenyltetrazolium chloride or TTC [13]. This stain, which marks viable cells based on enzymatic activity, has previously been used to measure tissue necrosis from ultrasound ablation in prostate and liver as well as interstitial thermal ablation in VX2 tumor [13]–[15]. These spatial maps of tissue viability allow direct evaluation of ablation success for complete tumor cross sections, as described below.

D. In vivo *ablation experiments*

The preclinical studies reported here were performed in open surgical procedures on rabbits with implanted VX2 liver tumors. Animals were anesthetized and opened via laparotomy. The probe assembly, including the cooling and circulation apparatus, was placed on the rabbit liver lobe surface and fixed by a 3D positioning arm (Medical Intelligence), as shown in Fig. 1(c). Acoustic coupling between the probe and liver surface was augmented by physiologic saline as needed.

Ablation exposures employed unfocused, 4.8 MHz continuous-wave ultrasound firing from the entire 32 element, 2.3×20 mm^2 aperture. Instantaneous acoustic power, calibrated by radiation-force balance measurements for the excitation voltages employed, was 9.6–19.2 W for the twelve exposures reported here, corresponding to 20.8–41.7 W/cm^2 acoustic energy density at the array surface. Duty fractions employed in these trials were either 85% or 100% (continuous wave). Using simulation of the diffracted field of the 32-element aperture [7], this range of surface intensities and duty cycles was found to correspond to *in situ* spatial-peak, temporal-average intensites 38.7–77.7 W/cm^2. Single exposures were performed for sonication times 20–120 s,

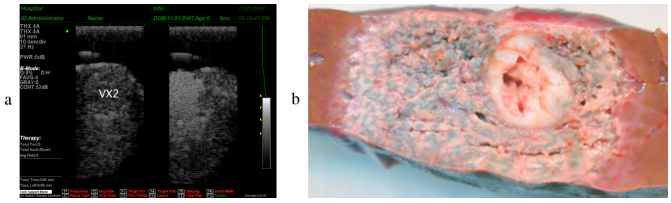

Fig. 5: Image-guided ablation of VX2 tumor in rabbit liver. (a) B-scan images from a THX4A probe before and after *in vitro* ablation using the same probe. (b) TTC-stained cross section of rabbit liver and VX2 tumor, showing complete *in vivo* tumor ablation.

with the goal of completely ablating a cross section of the VX2 tumor.

In vivo ablation results were quantitatively assessed by H&E histologic and TTC vital stains. For cross sections stained by TTC, ablation areas were quantified by manual segmentation of the region showing no TTC uptake (ImageJ, National Institutes of Health) [13]. Ablation volumes were estimated from the ablated area measured on TTC-stained tissue cross sections, using using volume-area ratios computed from thermal lesion geometry in previously validated simulations (Fig. 3).

III. Results

Image quality for B-scans of liver tissue and VX2 tumor using our 3 mm, 4.8 MHz, miniaturized array configuration is illustrated in Figs. 4(b) and 5(a). Fig. 4(b) compares B-scans of a typical VX2 tumor from a diagnostic-quality, 7 MHz, 192 element linear array (L7, Ardent Sound) and from a THX4A array. These images show the capability of the THX4A arrays to resolve tissue structure, including tumor boundaries and inhomogeneous internal tumor structure, in a manner suitable for targeting of interstitial ultrasound ablation. Notably, contrast achievable with the THX4A array at 4.8 MHz is comparable to that obtained with a 7 MHz diagnostic-quality linear array. Fig. 5(a) shows B-scans taken by a THX4A image-ablate array, before and after *in vitro* ablation of a VX2 tumor in rabbit liver. The post-treatment image shows vaporization visible as hyperechoic, transient image changes, suggesting that quantitative imaging of transient variations in tissue scattering [16] may be suitable for monitoring of treatments using these miniaturized image-ablate arrays.

Histologic confirmation of successful VX2 tumor ablation has been obtained both by TTC vital staining methods, illustrated in Figs. 4 and 5, and by standard hematoxylin and eosin (H&E) staining. Typical results from H&E staining for tissue ablated *in vivo* are shown in Fig. 6 for both normal rabbit liver tissue and for VX2 liver cancer. In both cases, bulk ultrasound ablation is seen to result in drastic structural changes associated with thermal coagulative necrosis.

Statistical evaluation of *in vivo* VX2 ultrasound ablation treatments is illustrated in Fig. 7. A total of 12 VX2 ablation trials were conducted with THX4A arrays and the unfocused 4.8 MHz exposures described above, covering a range of exposure times and intensities. Complete ablation of a tumor cross section was confirmed by TTC vital staining in 7 of 12 cases, strongly dependent on exposure conditions. For

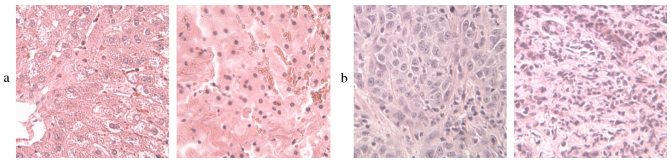

Fig. 6: Histology of rabbit liver and VX2 tumor ablated by THX4 array probes. (a) H&E stains of untreated (left) and ablated (right) normal liver tissue. (b) H&E stains of untreated (left) and ablated (right) VX2 tumor.

the frequency and aperture conditions investigated here, a threshold for successful ablation of a complete cross section was empirically determined as 747 J absorbed acoustic energy, as illustrated in Fig. 7(a). This energy threshold is easily achievable by the THX4A array design with sonication of duration 2 min or less, sufficient to overcome perfusion-induced heat losses in the liver.

Evaluation of bulk ablation efficiency is illustrated in Fig. 7(b), which shows estimated ablation volume vs. total delivered treatment energy for the 12 trials. These results show the expected trend of increasing ablation volume with absorbed acoustic energy ($r = 0.60$, $p = 0.037$), and are also consistent with a threshold for significant tissue ablation in the 500–1000 J range. The average volumetric ablation rate across all 12 experiments was 0.83 ± 0.34 ml/min, corresponding to mean ablation time of 40 min for a spherical 4 cm diameter defect. However, the achievable ablation rate was limited in these experiments by the small size of rabbit liver lobes (typical thickness 1.0–1.5 cm). Based on *in vitro* ablation results, corresponding *in vivo* ablation rates in larger tissue volumes are expected to exceed 2 ml/min with ablation depths >20 mm.

Selectivity of treatment was evaluated by comparison of thermal ablation margins in the azimuthal (array) direction with target values. For ablation with a 20 mm unfocused aperture, expected azimuthal width of the thermal ablation defect based on simulation results is 22 mm. For the 6 exposures with energy delivery above the empirical 747 J threshold for full ablation, measured widths of the thermal lesion were 22.0 ± 2.0 mm, in good agreement with the predicted width. In all cases, thermal ablation extended $\leq$4 mm beyond the planned margin in azimuth.

IV. Conclusion

These experiments show the feasibility of performing *in vivo* ablation of liver cancer using miniaturized, image-ablate ultrasound arrays. Experimental results demonstrate the capability of these devices to achieve ablation more efficient than high-intensity focused ultrasound, with treatment selectivity and control superior to radiofrequency ablation. A therapeutic platform based on these devices has potential to improve minimally-invasive management of liver cancer in the clinical setting.

Acknowledgment

This work was supported by NIH grant R43 CA124283.

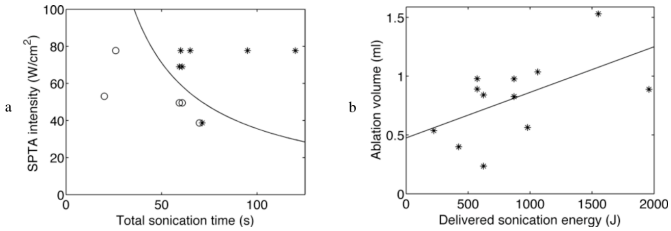

Fig. 7: Summarized *in vivo* VX2 ablation results for THX4A image-ablate probes. (a) Energy threshold for complete tumor ablation. SPTA in situ intensity is plotted vs. total sonication time for 12 *in vivo* VX2 ablation trials, with solid circles indicating ablation of a complete tumor cross section, open circles indicating incomplete ablation, and the empirical threshold line at 747 J total absorbed energy. (b) Plot of total ablation volume vs. absorbed acoustic energy for the same 12 *in vivo* VX2 ablation trials.

References

[1] Lafon C, Melodelima D, Salomir R, Chapelon JY. Interstitial devices for minimally invasive thermal ablation by high-intensity ultrasound. Int J Hyperthermia 2007; 23:153–163.

[2] Diederich CJ, Nau WH, Stauffer PR. Ultrasound applicators for interstitial thermal coagulation. IEEE Trans Ultrason Ferroelectr Freq Control 1999; 46:1218-1228.

[3] Lafon C, de Lima DM, Theillire Y, Prat F, Chapelon JY, Cathignol D. Optimizing the shape of ultrasound transducers for interstitial thermal ablation. Med Phys 2002; 29:290-297.

[4] Barthe PG, Slayton MH. Efficient wideband linear arrays for imaging and therapy. IEEE Ultras Symp 2000; 1249–1252.

[5] Chopra R, Bronskill MJ, Foster FS. Feasibility of linear arrays for interstitial ultrasound thermal therapy. Med Phys 2000; 27:1281-1286.

[6] Makin IRS, Mast TD, Faidi W, Runk MM, Barthe PG, and Slayton MH. Miniaturized ultrasound arrays for interstitial ablation and imaging. Ultras Med Biol 2005; 31:1539–1550.

[7] Mast TD. Fresnel approximations for ultrasonic fields of rectangularly symmetric sources. J Acoust Soc Am 2007; 121:3311–3322.

[8] Mast TD, Makin IRS, Faidi W, Runk MM, Barthe PG, Slayton MH. Bulk ablation of soft tissue with intense ultrasound: modeling and experiments. J Acoust Soc Am 2005; 118:2715–2724.

[9] Barthe PG, Slayton MH, Jaeger PM, Makin IRS, Gallagher LA, Mast TD, Runk MM, Faidi W. Ultrasound therapy system and ablation results utilizing miniature imaging/therapy arrays. IEEE Ultras Symp 2004; 1792–1795.

[10] Prat F, Centarti M, Sibille A, Abou el Fadil FA, Henry L, Chapelon JY, Cathignol D. Extracorporeal high-intensity focused ultrasound for VX2 liver tumors in the rabbit. Hepatology 1995; 21:832–836.

[11] Sasaki K, Medan MS, Azuma T, Kawabata K, Shimoda M, Umemura S. Effect of echo-guided high-intensity focused ultrasound ablation on localized experimental tumors. J Vet Med Sci 2006; 68:1069–1074.

[12] Frieser M, Schaber S, Strobel D, Bernatik T, Wehr H, Peters A, Hahn EG, Haensler J. Prolonged survival through combined treatment with radiofrequency ablation/ethanol instillation compared with radiofrequency ablation alone in the VX2 rabbit liver tumour model. Ultraschall Med 2007; 28:176–180.

[13] Karunakaran CP, Burgess MT, Holland CK, Mast TD. Role of cavitation in bulk ultrasound ablation: a histologic study. Proceedings of 8th International Symposium on Therapeutic Ultrasound (American Institute of Physics Conference Proceedings, 2009).

[14] Nau WH, Diederich CJ, Ross AB, Rieke V, Butts K, Sommers G. Evaluation of endorectal and urethral cooling devices during MR-guided ultrasound thermal ablation in canine prostate. Conf Proc IEEE Eng Med Biol Soc 2004; 4:2492-2495.

[15] Shafirstein G, Hennings L, Kaufmann Y, Novak P, Moros EG, Ferguson S, Siegel E, Klimberg SV, Waner M, Spring P. Conductive interstitial thermal therapy (CITT) device evaluation in VX2 rabbit model. Technol Cancer Res Treat 2007; 6:235–246.

[16] Mast TD, Pucke DP, Subramanian SE, Bowlus WJ, Rudich SM, Buell JF. Ultrasonic monitoring of *in vitro* radiofrequency ablation by echo decorrelation imaging. J Ultras Med 2008; 27:1685–1697.